Synthesis and Characterization of $MoSe_2$ and WSe_2 Nanoclusters

J. M. Huang† and D. F. Kelley*

Department of Chemistry, Kansas State University, Manhattan, Kansas 66506-3701

Received March 21, 2000
Revised Manuscript Received July 20, 2000

Several different types of semiconductor particles exhibiting quantum confinement have been synthesized and characterized, and in some cases, their photophysics have been extensively studied.[1] The most thoroughly studied are CdS and CdSe. Methods for the synthesis and surface derivatization of these nanoclusters are very well developed.[2−11] Nanoclusters of other materials, such as GaAs,[12] GaP,[13] InP,[14] and PbI_2[15] have also been examined. Comparatively, little work has been done on nanoclusters of the group VI transition metal dichalcogenides (MoS_2, WS_2, $MoSe_2$, and WSe_2). The synthesis and characterization of MoS_2 and WS_2 nanoclusters have been reported,[16,17] and we have recently reported on some of the photophysics and interfacial electron-transfer dynamics of these nanoclusters.[18−21] In this communication, we report the synthesis and characterization of $MoSe_2$ and WSe_2 nanoclusters. These nanoclusters are of interest in their own right and because of their comparison to the corresponding sulfides. One significant difference between the bulk selenides and the sulfides is in the phonon frequencies.[22] The selenides have significantly lower frequency vibrations that can affect the rates of radiationless processes such as trapping, band edge radiationless decay, and interfacial electron transfer.

The bulk forms of these materials are of considerable interest because of their possible application in photoelectrochemical cells. All of these materials crystallize into a hexagonal layered structure ($P6_3/mmc-D^4_{6h}$), with similar lattice constants.[23] This layered structure consists of covalently bound X−M−X, (M = Mo, W; X = S, Se) trilayers, separated by a relatively large van der Waals gap. The chalcogenide layers are two-dimensional hexagonal close-packed sheets, with the chalcogenide atoms of one layer directly above those of the layer on the other side of the metal layer. The metal atoms are in trigonal prismatic sites between the chalcogenide layers. The electronic structures of all of these materials are qualitatively similar, and all are indirect band gap semiconductors. Bandedge excitation corresponds largely to a metal-centered d−d transition.[24] $MoSe_2$ and WSe_2 have lowest indirect band gaps of 1.09 and 1.20 eV, respectively, as determined by photocurrent spectroscopy.[25] Both $MoSe_2$ and WSe_2 have lowest direct band gaps of 1.35 eV. These values are slightly smaller than those reported for the corresponding sulfides.[25]

Several different sizes of MoS_2 nanoclusters have been reported, ranging from 2.5 to 4.5 nm in diameter.[16] The absorption spectra of the smallest nanoclusters show strong quantum confinement, with the lowest direct absorption shifting from 680 nm for bulk MoS_2 to 360 nm in the 2.5-nm nanoclusters. X-ray diffraction of aggregated nanoparticles showed the same crystal structure as the bulk material. These studies did not assess the nanocluster morphology. The absorption spectrum of WS_2 nanoclusters is quite similar to what is observed for the smallest MoS_2 nanoclusters, having a lowest absorption maximum at 364 nm.[17] TEM images showed these nanoclusters to have diameters of about 4−9 nm, which is consistent with the ≈7-nm sizes deduced from rotational diffusion times. These studies were also able to infer the nanocluster morphology. Electron diffraction results showed that rings assigned to reflections along the *z*-axis were absent, indicating a lack of *z*-axis ordering. Specifically, the (0,0,2) ring, which is the most intense ring in the bulk WS_2 diffrac-

* To whom correspondence should be addressed. E-mail: dfkelley@ksu.edu.
† Present address: NSF/Center for Micro-Engineered Materials, 203 Farris Engineering Center, University of New Mexico, Albuquerque, New Mexico 87131.

(1) For a comprehensive review see: *Semiconductor Nanoclusters—Physical, Chemical and Catalytic Aspects*; Kamat, P. V., Meisel, D., Eds.; Elsevier: New York, 1997; also see the special issue on nanoscale materials, *Acc. Chem. Res.* **1999**, *32*.
(2) Murray, C. B.; Norris, D. J.; Bawendi, *J. Am. Chem. Soc.* **1993**, *115*, 8706.
(3) Spanhel, L.; Haase, M.; Weller, H.; Henglein, A. A. *J. Am Chem. Soc.* **1987**, *109*, 5649.
(4) Eychmüller, A.; Mews, A.; Weller, H. *Chem. Phys. Lett.* **1993**, *208*, 59. Mews, A.; Eychmüller, A.; Giersig, M.; Schooss, D.; Weller, H. *J. Phys. Chem.* **1994**, *98*, 934.
(5) Eychmüller, A.; Hässelbarth, A.; Katsikas, L.; Weller, H. *Ber. Bunsen-Ges. Phys. Chem.* **1991**, *95*, 79.
(6) Hines, M. A.; Guyot-Sionnest, P. *J. Phys. Chem.* **1996**, *100*, 468.
(7) Danek, M.; Jensen, K. F.; Murray, C. B.; Bawendi, M. G. *Chem. Mater.* **1996**, *8*, 173.
(8) Rogach, A. L.; Kornowski, A.; Gao, M.; Eychmuller, A.; Weller, H. *J. Phys. Chem. B* **1999**, *103*, 3065.
(9) Peng, X.; Schlamp, M. C.; Kadavanich, A. V.; Alivisatos, A. P. *J. Am. Chem. Soc.* **1997**, *119*, 7019.
(10) Tian, Y.; Newton, T.; Kotov, N. A.; Guldi, D. M.; Fendler, J. H. *J. Phys. Chem.* **1996**, *100*, 8927.
(11) Dabbousi, B. O.; Rodriguez-Viejo, J.; Mikulec, F. V.; Heine, J. R.; Mattoussi, H.; Ober, R.; Jensen, K. F.; Bawendi, M. G. *J. Phys. Chem. B* **1997**, *101*, 9463.
(12) Olshavsky, M. A.; Goldstein, A. N.; Alivasatos, A. P. *J. Am. Chem. Soc.* **1990**, *112*, 9438.
(13) Micic, O. I.; Sprauge, J. R.; Curtis, C. J.; Jones, K. M.; Machol, J. L.; Nozik, A. J. *J. Phys. Chem. B* **1995**, *99*, 7754.
(14) Kim, S.-H.; Wolters, R. H.; Heath, J. R. *J. Chem. Phys.* **1996**, *105*, 7957. Micic, O. I.; Gheong, C. H.; Fu, H.; Zunger, A.; Sprauge, J. R.; Mascarenhas, A.; Nozik, A. J. *J. Phys. Chem. B* **1997**, *101* 4904.
(15) (a) Sengupta, A.; Jiang, B.; Mandal, K. C.; Zhang, J. Z. *J. Phys. Chem. B* **1999**, *103*, 3128. (b) Micic, O. I.; Zongguan, L.; Mills, G.; Sulivan, J. C.; Meisel, D. *J. Phys. Chem.* **1987**, *91*, 6221.
(16) (a) Wilcoxon, J. P.; Samara, G. A. *Phys. Rev. B* **1995**, *51*, 7299. (b) Wilcoxon, J. P.; Newcomer, P. P.; Samara, G. A. *J. Appl. Phys.* **1997**, *81*, 7934.
(17) Laitinen, R. A.; Huang, J. M.; Kelley, D. F. *Phys. Rev. B*, in press.
(18) Parsapour, F.; Kelley, D. F.; Craft, S.; Wilcoxon, J. P. *J. Chem. Phys.* **1996**, *104*, 4978.
(19) Doolen, R.; Laitinen, R.; Parsapour F.; Kelley, D. F. *J. Phys. Chem. B* **1998**, *102*, 3906.
(20) Huang, J. M.; Kelley, D. F. *J. Chem. Phys.* **2000**, *113*, 793.
(21) Chikan, V.; Waterland, M. R.; Huang, J. M.; Kelley, D. F. *J. Chem. Phys.*, in press.
(22) *Electrons and Phonons in Layered Crystal Structures*; Wieting, T. J., Schluter, M., Eds.; Reidel: Dordrecht, Holland, 1979.
(23) Levy, F. *Crystallography and Crystal Chemistry of Materials with Layered Structures*; Reidel: Dordrecht, Holland, 1976; p 2.
(24) Coehoorn, R.; Haas, C.; Dijkstra, J.; Flipse, C. J. F.; deGroot, R. A.; Wold, A. *Phys. Rev. B* **1987**, *35*, 6195, 6203. Evans, B. L.; Young, P. A. *Proc. R. Soc. A* **1965**, *284*, 402.
(25) Kam K. K.; Parkinson, B. A. *J. Phys. Chem.* **1982**, *86*, 463.

10.1021/cm0002517 CCC: $19.00
Published on Web 09/13/2000

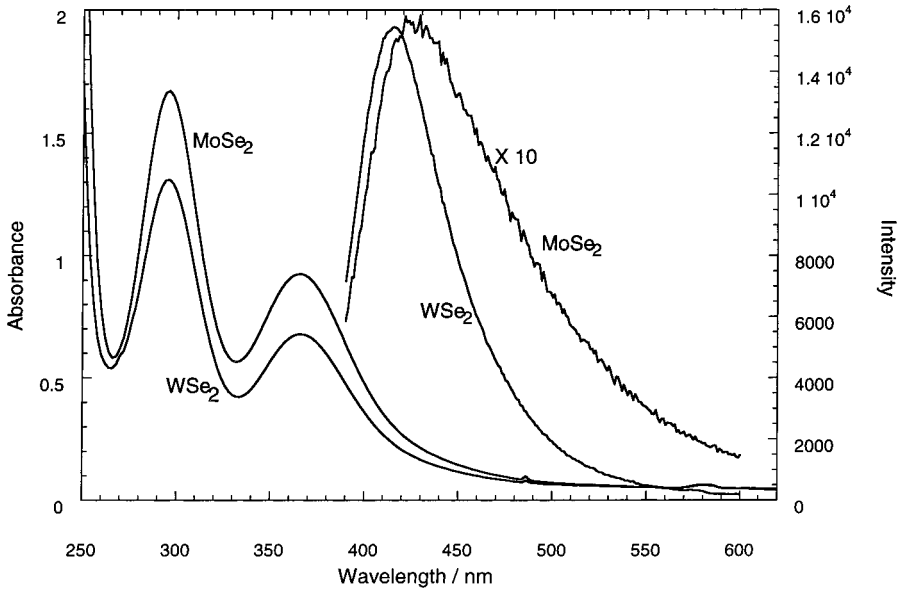

Figure 1. Absorption and emission spectra of $MoSe_2$ and WSe_2 nanoclusters. The emission spectra were obtained with 312-nm excitation.

tion pattern, was not observed. Comparison with crystallographic calculations for various thicknesses indicates that these nanoclusters consist of single S−W−S trilayers. This conclusion makes good sense; only weak van der Waals forces hold the trilayers together in the bulk material.

$MoSe_2$ and WSe_2 nanoclusters are synthesized using methods very similar to those used to synthesize MoS_2 and WS_2 in refs 16 and 17. This method involves dissolving the metal(IV) chloride in an anhydrous inverse micelle and adding H_2Se. $MoCl_4$ is synthesized from $MoCl_5$ (obtained from Aldrich). This synthesis involves refluxing $MoCl_5$ in tetrachloroethylene for about 3 days in a sealed, oxygen-free vessel. Following reaction, the solid is allowed to settle, the tetrachloroethylene is pipetted and pumped off, and the resulting solid is repeatedly washed with CCl_4 in an inert atmosphere drybox. Tungsten(IV) chloride was obtained from Aldrich and was repeatedly washed with carbon tetrachloride in an inert atmosphere drybox to remove undesired tungsten oxychlorides. The resulting $MoCl_4$ or WCl_4 is then dissolved in a degassed ternary tridodecylmethylammonium iodide (TDAI)/hexanol/octane (8/8/84 by weight) inverse micelle solution, at a concentration of $\approx 1.0 \times 10^{-3}$ M. All solvents are thoroughly dried prior to preparing the micelle solutions. Several hours are allowed to ensure complete dissolution. To this rapidly stirring solution was added ≈4.0 molar equiv of H_2Se via a gastight syringe. The H_2Se is generated by the reaction of Al_2Se_3 with H_2SO_4 in a vacuum line. Following H_2Se addition, the mixture is allowed to stir for 30 min. The resulting nanoclusters in the inverse micelle solution are then extracted with an equal volume of acetonitrile. The nanoclusters partition between the nonpolar octane phase and the polar acetonitrile/TDAI/hexanol phase, with most going into the polar phase. Similar behavior has been observed for MoS_2 and WS_2 nanoclusters. The nanoclusters in both phases are stable with respect to air and small amounts of water.

The absorption and emission spectra of $MoSe_2$ and WSe_2 nanoclusters in acetonitrile are shown in Figure 1. The nanoclusters that remain in the octane phase exhibit an absorption spectrum that is essentially identical to those that extract into the polar phase. This is an important point because the acetonitrile-soluble and octane-soluble nanoclusters presumably have different surface charges. This result thus implies that the observed absorption spectra are due to transitions in the nanocluster, rather than to surface excited states. The absorption spectra are remarkably similar to each other, both showing a lowest absorption maxima at 366 nm. These spectra are also quite similar to the spectra obtained for MoS_2 and WS_2 nanoclusters, with the selenide spectra being shifted only a few nanometers to the red. We note that these spectra are also similar to those obtained in the case of PbI_2 nanoclusters. Assignment of the PbI_2 spectra has been controversial. It has been suggested that the analogous peaks in the PbI_2 case may be assigned to ionic species such as I_3^-, rather than to the nanoclusters, and counterarguments have been given.[15] Independent of any controversy in the PbI_2 case, the results of blank and acetonitrile extraction experiments rule out such an assignment in the present cases. Specifically, performing the synthesis without the metal chloride results in no 295- or 366-nm peaks. Furthermore, it is possible to generate I_3^- by the addition of a small amount of I_2 to the micelle solution. Upon extraction with acetonitrile, I_3^- goes entirely into the acetonitrile phase. In contrast, we find that, upon acetonitrile extraction of the micelle/nanocluster solution, a significant fraction of the $MoSe_2$ and WSe_2 nanoclusters go into the octane phase. While these experiments show that the 366-nm absorption peak is due to the nanoclusters, they do not exclude the possibility that some of this absorption is due to surface states. The emission spectrum of WSe_2 peaks somewhat to the blue and is an order of magnitude more intense than that of $MoSe_2$. These spectral and intensity differences are due to differences in the relaxation and carrier trapping dynamics and/or differences in the emitting state in some fraction of the nanoclusters. These dynamics will be discussed in a later paper.

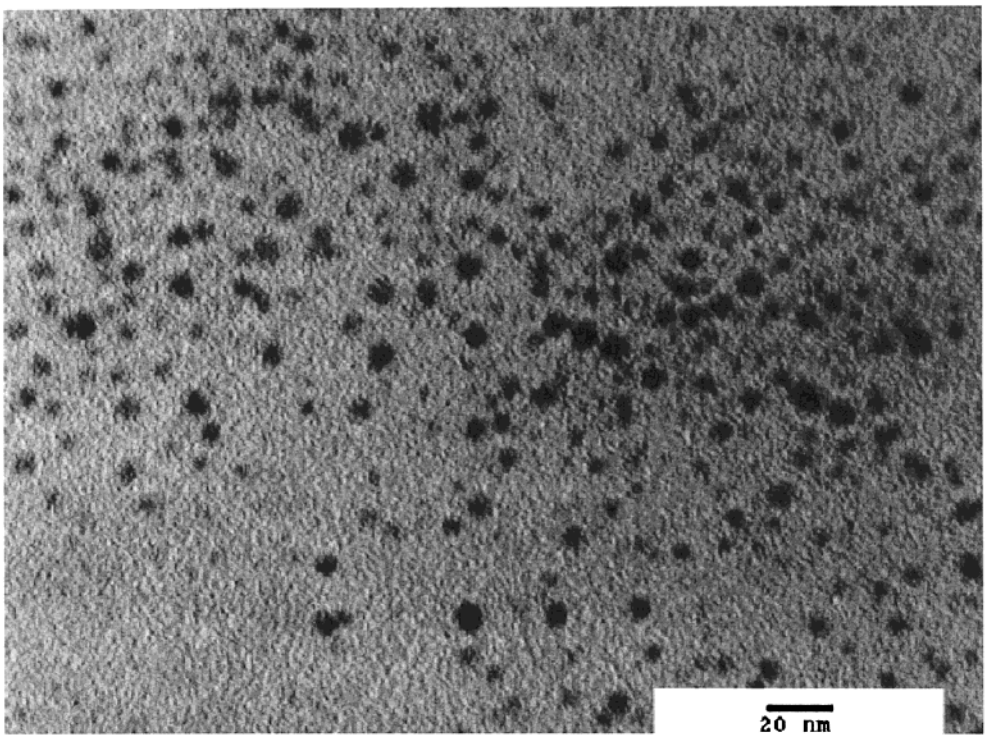

Figure 2. TEM images of $MoSe_2$ nanoclusters.

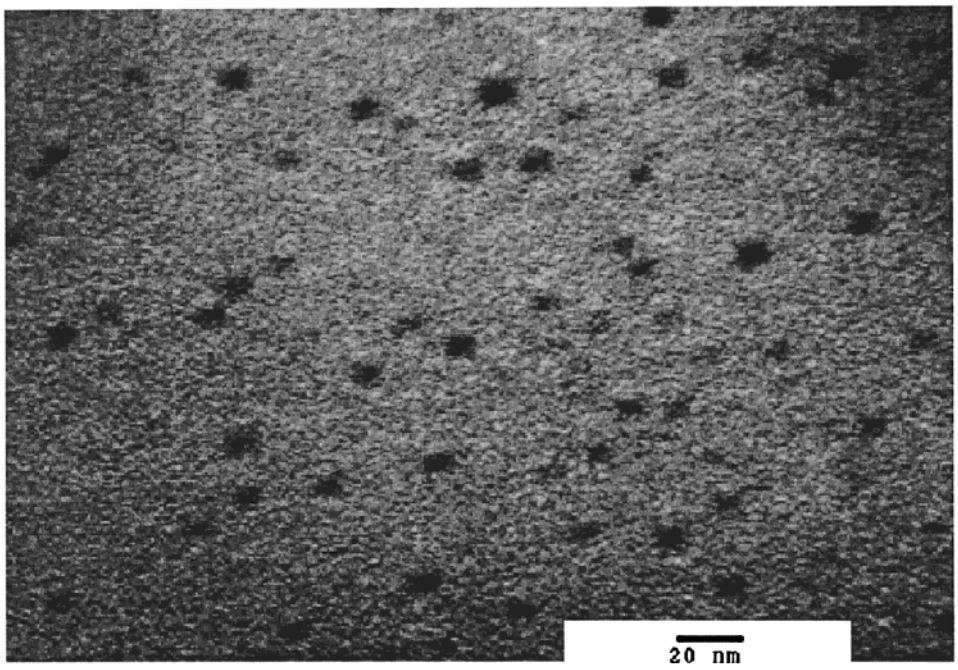

Figure 3. TEM images of WSe_2 nanoclusters.

TEM images and electron diffraction results were obtained on a Philips CM-100 transmission electron microscope. Samples were prepared by diluting the nanocluster octane solution (following extraction with acetonitrile) by a factor of 5 with octane and evaporating a drop onto a Formvar grid. These samples contain very little TDAI, which interferes with the TEM imaging and electron diffraction. TEM images of the $MoSe_2$ and WSe_2 nanoclusters are shown in Figures 2 and 3, respectively. The images show that, in both cases, there is some polydispersity of the particle sizes. The $MoSe_2$ particles have diameters of about 3.5−6 nm. The WSe_2 particles are, on average, slightly larger, with diameters of about 4−7 nm.

An electron diffraction pattern of WSe_2 nanoclusters and the assignments of the diffraction rings are shown in Figure 4. The diffraction "rings" consist of concentric sets of spots due to the finite number of nanoclusters in the electron beam focus. The assignments of the very weak (barely visible) spots at larger diffraction angles than the (2,0,0) ring are somewhat ambiguous and are not given. An almost identical diffraction pattern is obtained for $MoSe_2$. The assignments shown in Figure 4 correspond to bulk WSe_2 with one important excep-

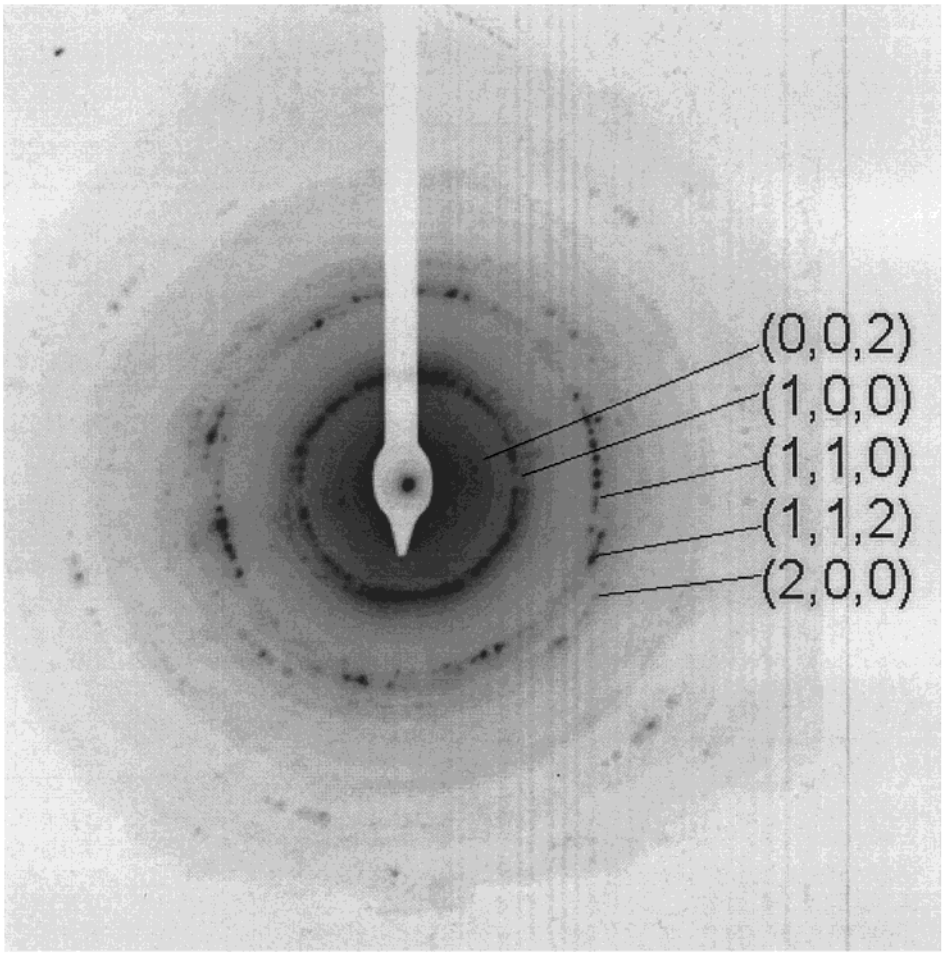

Figure 4. Electron diffraction pattern from WSe_2 nanoclusters. The assignments of the diffraction rings are also indicated.

tion. The (0,0,2) ring, which is the most intense ring in bulk WSe_2, is almost completely absent in the nanoclusters. These results were compared to the calculated diffraction patterns calculated for various nanocluster diameters and thicknesses. The calculated patterns show that the most intense ring is due to the (0,0,2) refection whenever the nanocluster is more than one trilayer thick. However, the experimentally observed diffraction pattern shows that this ring is almost completely absent. This is the same situation as was observed in the WS_2 nanoclusters, and the same interpretation is applicable here. We conclude that the $MoSe_2$ and WSe_2 nanoclusters have disk morphologies; they consist of single trilayer sheets. The very weak spots corresponding to the (0,0,2) ring are probably due to some aggregation that occurs when the sample is evaporated onto the Formvar grid.

These nanoparticles provide interesting systems for the study of relaxation, carrier trapping, and interfacial electron transfer dynamics. We are currently using time-resolved optical spectroscopy to study these dynamics, and the results will be reported in later papers. However, perhaps the most remarkable aspect of all of these nanoclusters (MoS_2, WS_2, $MoSe_2$, and WSe_2) is the similarity of the absorption spectra. They all show their first absorption maxima in the 360−366-nm region. This observation is independent of the exact synthetic conditions. For example, variation of the ternary micelle composition over the entire range for which a single micelle phase is formed (i.e., variation of the TDAI:octane ratio by over a factor of 5 or the TDAI:hexanol ratio by over a factor of 2) results in identical spectra. This suggests that the nanocluster size distribution may be controlled by thermodynamics, rather than by nucleation and growth kinetics. Furthermore, the observations that the absorption spectra are well resolved while the nanocluster samples are somewhat polydisperse suggest that the absorption spectrum does not change with nanocluster size as predicted by simple quantum confinement theory. This may be due to the observed transition being along the crystallographic *c*-axis (and therefore insensitive to the extent of $x-y$ quantum confinement) or some of the 366-nm absorption being due to surface states. The extent to which the nanocluster size distribution varies with these variations in micelle composition and the extent to which the absorption spectrum varies with nanocluster size are currently being studied and will be reported in later papers.

Acknowledgment. The authors would like to thank Professor Christer Aakeroy for his help in analyzing the electron diffraction results and Dr. Daniel Boyle for his help in obtaining the TEM images. This work was supported by a grant from the U.S. Department of Energy (Grant DE-FG03-96ER14717).

CM0002517